

Unsteady wetting of soft solids

Surjyasish Mitra^{1*}, Quoc Vo^{2*}, Marcus Lin² & Tuan Tran²

¹*School of Physical and Mathematical Sciences, Nanyang Technological University, 50 Nanyang Avenue, 639798, Singapore.*

²*School of Mechanical & Aerospace Engineering, Nanyang Technological University, 50 Nanyang Avenue, 639798, Singapore.*

**These authors contributed equally.*

From hydrogels and plastics to liquid crystals, soft solids cover a wide array of synthetic and biological materials ¹ that play key enabling roles in advanced technologies such as 3D printing ², soft robotics ³, wearable electronics ⁴, self-assembly ⁵, and bioartificial tissues ^{6,7}. Their elasticity and stimuli-induced changes in mechanical, optical, or electrical properties offer an unique advantage in designing and creating new dynamically functional components for sensing, micro-actuation, colour changes, information and mass transport. To harness the vast potential of soft solids through their ability to respond to the environment, a thorough understanding of their reactions when exposed to liquids is needed. Attempts to study the interactions between soft solids and liquids have largely focused on the wetting of soft solids ⁸⁻¹² and its resulting deformation at equilibrium ^{12,13}, in quasi-static state ¹⁴, or in steady state ^{15,16}. Here we consider the frequently encountered case of unsteady wetting of a liquid on a soft solid, and show that transient deformation of the solid is necessary to understand unsteady wetting behaviours. We find that the initial spreading of the liquid occurs unin-

terrupted in the absence of solid deformation. This is followed by intermittent spreading, in which transient deformation of the solid at the three-phase contact line (CL) causes alternation between CL sticking and slipping. We identify the spreading rate of liquids and the viscoelastic reacting rate of soft solids the two competing factors in initiating intermittent spreading. We formulate and validate experimentally the conditions required for the contact line to transition from sticking to slipping. By considering the growing deformation of soft solids as dynamic surface heterogeneities, our proposed conditions for stick-slip transition in unsteady wetting on soft solids broaden the classical theory on wetting hysteresis on rigid solids. Our results provide a basis to understand dynamic responses of soft solids to unsteady wetting.

Wetting phenomena on soft solids has been studied extensively for the past few decades ^{8–12} owing to the increasingly central role of soft materials in advanced applications, from flexible electronics ⁴ and soft robotics ³ to biomedicine ^{6,7}. Majority of research focuses on wetting behaviours with the liquid spreading rate smaller than the solid reacting rate against the liquid-air interfacial tension at the spreading front. These behaviours are often observed at equilibrium ^{12,13}, in quasi-static state ¹⁴, or in steady state by forced contact line (CL) motion ^{15,16}. In contrast, unsteady wetting on soft solids is a more frequently encountered but much less explored situation, where unsteady liquid spreading is spontaneously driven by surface tension imbalance at the contact line without any external control on the spreading rate. In this case, CL displacement and formation of the so-called wetting ridge, i.e., solid deformation at the contact line, are both in transient states. The resulting intermittent CL motion in unsteady wetting is largely unexplored, as

opposed to its counter-part in quasi-static or forced wetting^{14–19}, and is therefore the focus of our study.

In this Article, we investigate intermittent spreading behaviour of unsteady wetting on soft solids. We let liquid droplets to spread freely when they are deposited on soft surfaces, thereby allowing the liquid to spread and interact with the developing wetting ridge without any external constraint. We find that for a wide range of liquid’s surface tension and solid’s elasticity, fast inertial spreading transitions to intermittent spreading, i.e., alternation between CL sticking and slipping, when the spreading rate reduces and becomes comparable to the viscoelastic reacting rate of the soft solid. The stick-slip spreading behaviour in this case consists of two essential elements, liquid spreading and wetting ridge formation, both in their transient states. Whenever the contact line (CL) sticks, it liberates itself and slips due to the combined effect of capillary force and flow inertia accumulated from the early inertial spreading.

Results

We perform numerous unsteady wetting experiments on soft substrates and characterise the spreading dynamics of liquids, focusing on the stick-slip behaviour before the liquids reach equilibrium (Methods). We track the contact radius r and the corresponding contact angle θ with respect to time t for liquids of varying surface tensions γ , from 38.7 Nm^{-1} to 72.2 Nm^{-1} , and solids with shear modulus G varying from 1.6 kPa to 501.9 kPa . In Fig. 1a, we show a representative experiment in which a 0.5 mm radius DI water droplet spreads on a soft substrate with $G = 1.6 \text{ kPa}$.

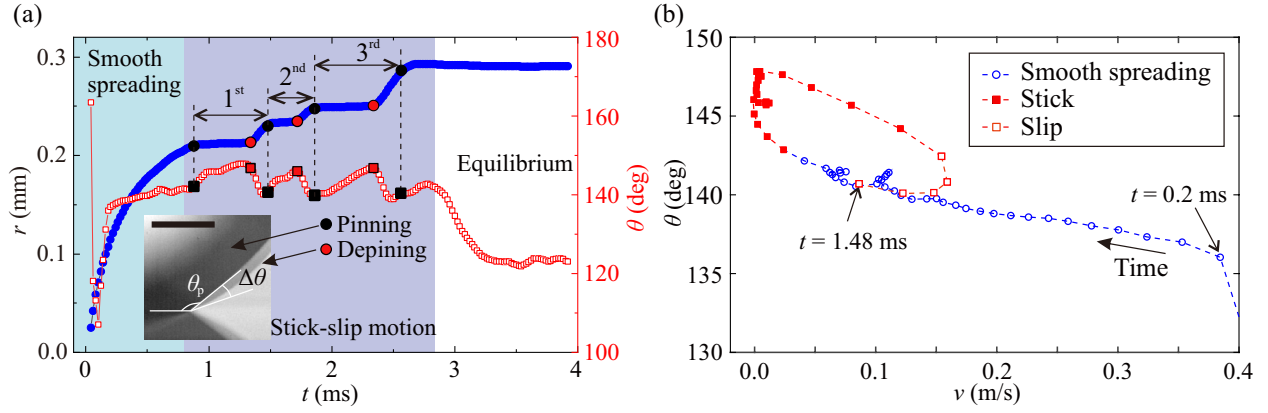


Figure 1: (a) Variation of droplet - solid footprint radius, i.e., the spreading radius r and dynamic contact angle θ over time t for a 0.5 mm radius water droplet spreading on a soft surface with $G = 1.6$ kPa. Inset: a superimposed image of the pinning and depinning snapshots of the third stick-slip event in the main plot. The scale bar represents 100 μm . (b) Plot showing the dependence of dynamic contact angle θ on the velocity v of the contact line for experiment shown in (a). Only the data corresponding to the smooth spreading phase (blue open circles), the first stick phase (closed red squares) and the first slip phase (open red squares) are shown.

In the initial spreading stage ($t \lesssim 0.88$ ms), the contact radius r increases without interruption while the contact line (CL) velocity gradually reduces from its peak value, a behaviour similar to the initial spreading of low viscosity liquids on rigid surfaces^{20,21}. The relatively high CL velocity (~ 1 m/s) generated by inertia-capillary balance leaves the soft surface insufficient time to deform and obstruct the CL motion²². In the subsequent stage (0.88 ms $\lesssim t \lesssim 2.66$ ms), the liquid spreads through several stick-slip cycles before it reaches an equilibrium and stops. Here, sticking occurs when either the entire contact line or part of it is pinned, causing an abrupt drop in CL velocity, whereas slipping occurs when the contact line depins and its velocity resumes. For instance, sticking is identified when r appears almost constant (Fig. 1a), although strictly speaking, the contact line does not completely halt as it is not simultaneously pinned. Slipping then occurs when the contact line progressively liberates itself from the pinned sites and moves with a velocity significantly higher than that during sticking.

To understand the stick-slip behaviour in unsteady wetting, we explore how it deviates from the one observed in quasi-static wetting, a simplified situation typically associated with low CL velocity. In a stick-slip cycle of unsteady wetting, the CL velocity v shifting from negligibly low to high is accompanied by the corresponding contact angle θ switching from increasing to decreasing. As a result, we detect a cyclic relation between θ and v (Fig. 1b), a contrasting behaviour to the monotonic increase of θ with v in quasi-static wetting¹⁷. Furthermore, we note that CL depinning in quasi-static wetting is triggered by capillary force due to the contact angle increase $\Delta\theta$ developed during CL sticking (inset of Fig. 1a)¹⁷. In unsteady wetting, however, depinning is triggered by both the capillary force and the flow inertia generated in the initial fast spreading

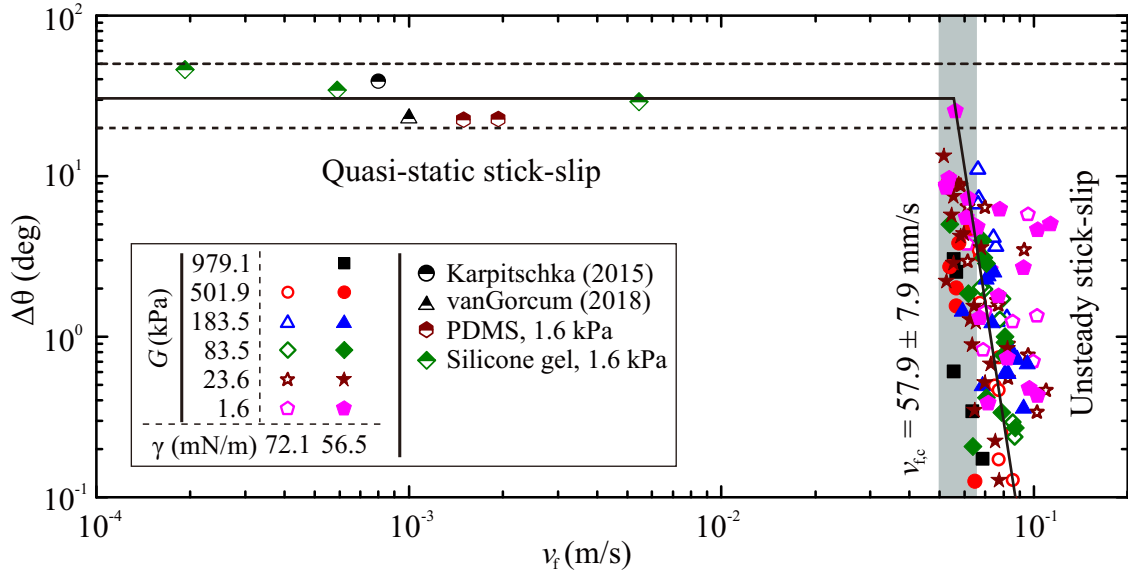


Figure 2: Variation of pinning-depinning transition contact angle $\Delta\theta$ on contact line velocity prior to pinning, v_s for 0.5 mm radius DI water and 5% ethanol-water mixture droplets exhibiting stick slip motion while spreading on soft PDMS surfaces with shear modulus in the range $1.6 \text{ kPa} \leq G \leq 979.1 \text{ kPa}$. Steady state $\Delta\theta$ values from inflation experiments (see Methods) and existing literature^{17,23} are shown for reference. The dashed lines show the range of values within which droplets exhibit contact angle hysteresis on PDMS.

stage. Indeed, an assessment of the relation between $\Delta\theta$ and the flow velocity v_f representing the flow inertia near the contact line (Methods) reveals a distinction between depinning mechanisms in quasi-static and unsteady wetting behaviours (Fig. 2). At small flow velocity ($v_f \lesssim 58$ mm/s), i.e., for quasi-static wetting, $\Delta\theta$ is approximately a constant comparable to the contact angle hysteresis, indicating that depinning is only dictated by the contact angle increase during sticking, not the flow near the contact line. This also suggests that the wetting ridge is fully developed before depinning^{14, 17–19}. At high flow velocity ($v_f > 58$ mm/s), i.e., for unsteady wetting, $\Delta\theta$ rapidly drops with increasing v_f , signifying a formidable role of flow inertia in causing depinning beside the capillary force. Moreover, since the contact line depins when $\Delta\theta$ in unsteady wetting is smaller than that in quasi-static wetting, we infer that depinning occurs in the transient state of wetting ridge formation.

We examine in greater details how depinning occurs when the wetting ridge is taking shape using bottom-view interferometric observations, shown in Fig. 3a. We note that a wetting ridge is undetectable before CL pinning, but starts growing as soon as CL pinning occurs ($t = 1.85$ ms), evidenced by the growing number of interference fringes from $t = 1.85$ ms to $t = 2.35$ ms (Fig. 3a and Supplementary Fig. 2). Depinning then is triggered at several weak and isolated pinned points, starting from $t = 2.35$ ms and then completing at $t = 2.41$ ms when the entire contact line displaces (Fig. 3a). Nonetheless, as the total duration for depinning is ≈ 0.05 ms, much shorter than the sticking duration (≈ 0.5 ms), it is reasonable to assume that depinning occurs instantaneously. This also implies that depinning is triggered only by the liquid flow and contact line conditions during sticking.

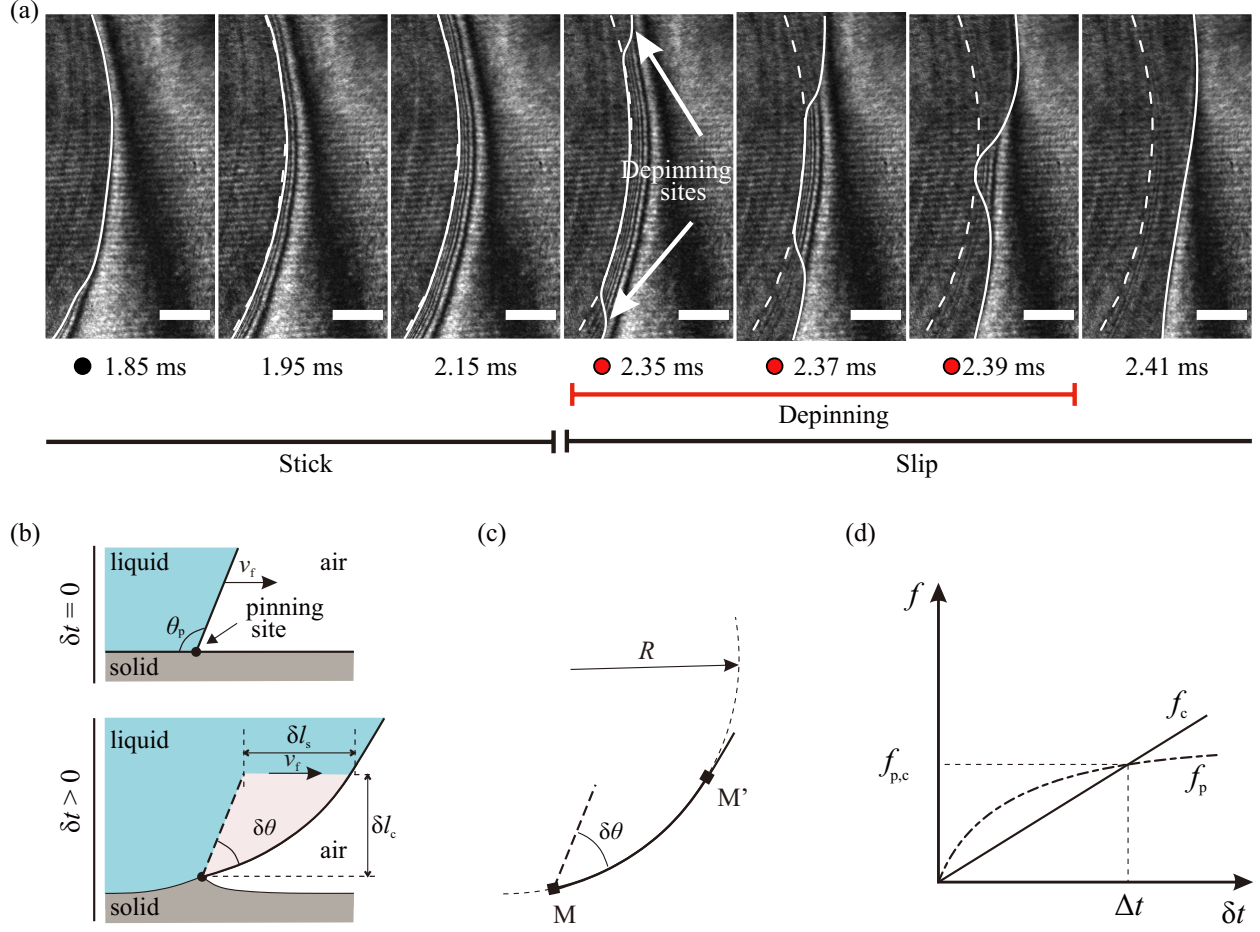


Figure 3: (a) Snapshots showing the bottom-view interferometric images of one typical stick-slip cycles. The scale bars represent $50 \mu\text{m}$. In each snapshot, the solid lines indicate the contact line positions at that moment, while the dashed lines represent the contact line at the pinning moment, i.e., $\delta t = 0$. (b) Schematics showing dynamical events at contact line during pinning-depinning cycles. (c) Force on the liquid-air interface during pinning. (d) Illustration showing the change in capillary force at the contact line f_c and the pinning force f_p with time δt . Depinning happens when the two curves meet, i.e., at $\delta t = \Delta t$ and $f_p = f_{p,c}$.

As a result, we seek to formulate the depinning condition in unsteady wetting by considering the force balance near the contact line at a small time δt after CL pinning. We denote θ_p the contact angle at pinning, i.e., when $\delta t = 0$. As the contact line is fixed but the liquid is still moving due to its inertia, the liquid-air interface near the contact line deforms, causing a contact angle increase $\delta\theta$ at $\delta t > 0$ (Fig. 3b). The vertical extent of the deformed interface is dictated by the capillary velocity $v_c \sim \gamma^{1/2}(\rho r_0)^{-1/2}$ and is estimated as $\delta l_c \sim v_c \delta t \sin \theta_p$. Here, ρ and r_0 are the density and the radius of the droplet, respectively. The liquid beyond δl_c continues moving unaffected by CL pinning with the flow velocity v_f . As a result, the liquid volume Ω slowed down by CL pinning is bounded vertically by δl_c and horizontally by $\delta l_s = v_f \delta t$, giving $\Omega \sim L \delta l_c \delta l_s$, where L is the length of the contact line. We estimate the corresponding deceleration of Ω as $v_f/\delta t$. This deceleration is caused by the capillary force (per unit length) $f_c \sim (\gamma/R)l_{MM'}$, in which the deformed interface has the radius of curvature R and length $l_{MM'} \approx (\delta\theta/\pi)R$ (see Fig. 3c). Thus, the force balance for the deceleration of Ω is written as $Lf_c \sim \rho\Omega v_f/\delta t$, or

$$\delta\theta \sim \pi \sin \theta_p \text{We} \frac{\delta t}{\tau_c}, \quad (1)$$

where $\tau_c = (\rho r_0^3/\gamma)^{1/2}$ is the inertial-capillary time, and $\text{We} = v_f^2 \rho r_0/\gamma$ is a Weber-like number comparing the flow inertia against capillarity. The linear relation between $\delta\theta$ and δt shown in Eq. 1 is consistent with our experimental observations for different liquids and shear moduli.

We stress that Eq. 1 holds at any moment during sticking, including the depinning moment, i.e., when $\delta t = \Delta t$ and $\delta\theta = \Delta\theta$. We recall that for depinning either on rigid surfaces or on soft surfaces in quasi-static condition, the capillary force increase associated with $\Delta\theta$ is required to overcome a fixed pinning force and is independent of the sticking duration Δt ^{17,24}. On the

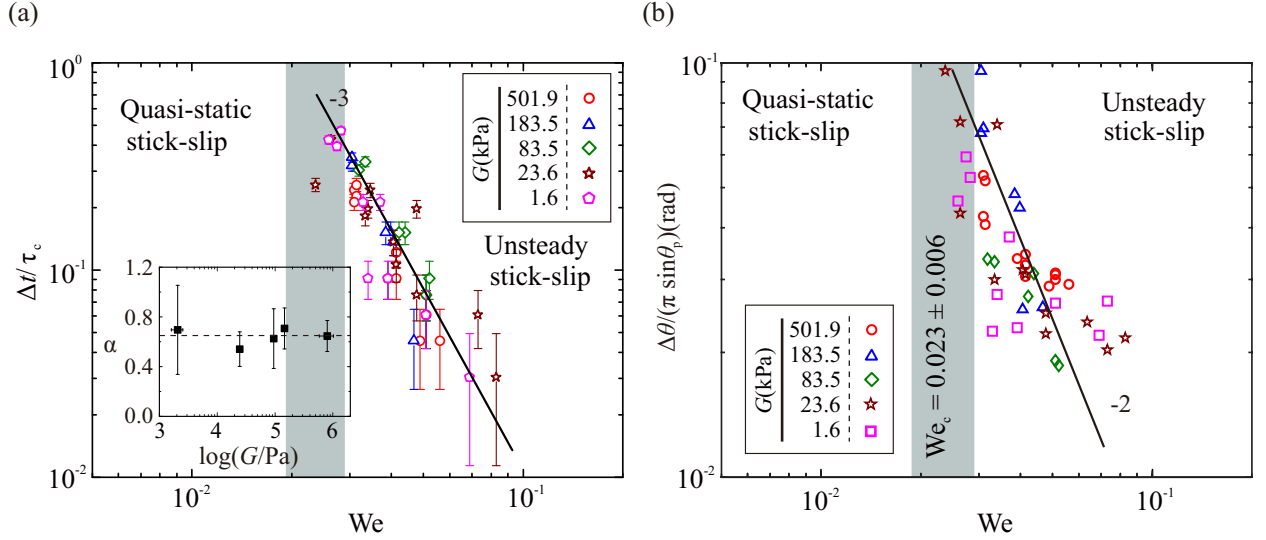


Figure 4: (a) Plot showing $\Delta t / \tau_c$ versus We . The solid line shows the scaling law $\Delta t / \tau_c \sim We^{-3}$, equivalently $\alpha = 2/3$. Inset shows variation of exponent α with static shear modulus G obtained by fitting the data in (a) to Eq. 3. α appears to be independent from G ; its average value is $\alpha \approx 0.65 \pm 0.07$. (b) Plot showing $\Delta \theta / (\pi \sin \theta_p)$ versus We . The solid line shows the scaling law $\Delta \theta / (\pi \sin \theta_p) \sim We^{-2}$, equivalently $\alpha = 2/3$. The shaded regions in (a) and (b) indicate the critical Weber number We_c which represents the transition between quasi-static and unsteady stick slip.

contrary, $\Delta\theta$ consistently increases with Δt in our experiment, indicating that the CL pinning force in unsteady soft wetting grows with time. Combining with the growth of ridge size during sticking (Fig. 3a), we infer that the pinning force increases with the pinning time δt following the growth in ridge size, which is finite at $\delta t = 0$. Here, the increase in ridge size is characterised by the soft solids's viscoelastic relaxation timescale $\tau_v = \eta_s/G$, where η_s is the dynamic viscosity of the soft solids²⁵. As a result, we approximate the pinning force (per unit length) at $\delta t > 0$ as $f_p \sim k(\delta t/\tau_v)^\alpha$, where α is a dimensionless constant; k has the dimension of force per unit length and plays a similar role to the contact-line spring constant in the classical theory of contact angle hysteresis²⁶. We note that the necessary condition to depin at a finite time is $\alpha < 1$ following the linear increase of f_c with δt shown in Eq. 1.

Depinning, therefore, is possible when the increase in capillary force (per unit length) $\gamma[\cos \theta_p - \cos(\theta_p + \Delta\theta)]$ becomes equal to the pinning force (per unit length) f_p , or $\gamma[\cos \theta_p - \cos(\theta_p + \Delta\theta)] \approx k(\Delta t/\tau_v)^\alpha$. Combining with Eq. 1 at depinning when $\delta t = \Delta t$ and $\delta\theta = \Delta\theta$, the depinning conditions for small $\Delta\theta$ become

$$\frac{\Delta t}{\tau_c} \sim \Phi \text{We}^{1/(\alpha-1)}, \text{ or } \frac{\Delta\theta}{\pi \sin \theta_p} \sim \Phi \text{We}^{\alpha/(\alpha-1)}, \quad (2)$$

where the dimensionless parameter Φ is

$$\Phi = \left(\frac{\pi\gamma \sin^2 \theta_p}{k} \right)^{1/(\alpha-1)} \left(\frac{\tau_v}{\tau_c} \right)^{\alpha/(\alpha-1)}. \quad (3)$$

We highlight that Eq. 2 explicitly predicts both the maximum duration Δt and the maximum contact angle increase $\Delta\theta$ from pinning to depinning. We experimentally test these predictions by showing $\Delta t/\tau_c$ and $\Delta\theta/(\pi \sin \theta_p)$ versus We in Fig. 4a and Fig. 4b, respectively. The experi-

mental data, comprising of all substrates with G varying from 1.6 kPa to 501.9 kPa, unequivocally agree with both power laws derived in Eq. 2 for $\alpha = 0.65 \pm 0.07$. The inset of Fig. 4a shows that α fluctuates around 0.65 (dashed line in the inset) for G varying almost three orders of magnitude, indicating that α can be practically considered constant in the explored range of shear modulus. The shaded areas in Fig. 4 indicate the critical Weber number $We_c = 0.023 \pm 0.006$ beyond which unsteady stick-slip happens (Methods). This excellent agreement thus confirms our theoretical model on the depinning condition for unsteady wetting on soft surfaces.

Discussions

Dynamic defects and soft contact line elasticity. The scaling law describing the pinning force on soft solids at the contact line (CL), $f_p \sim k(\delta t/\tau_v)^\alpha$ with $\alpha = 0.65 \pm 0.07 \approx 2/3$, is consistent with the classical theory on contact-line pinning²⁶ considering growing deformation on soft solids as dynamic surface heterogeneities.

For wetting on rigid surfaces, the widely accepted theory for contact-line pinning^{26–28} attributes surface defects of a fixed characteristic size ζ to causing CL pinning and subsequent deformation of the liquid-air interface. The maximum pinning force (per unit length) before depinning is calculated as $f_p \sim k_r \varepsilon_m$, where the parameter $k_r \sim \pi \gamma \sin^2 \theta_p / \ln(L'/\zeta)$ acts as a spring constant for elastic deformation of the liquid-air interface near the contact line. Here, L' is the upper-bound length scale of the CL region and is conveniently estimated using droplet size in the case of wetting by liquid droplets; the normalised amplitude ε_m at maximum deformation is estimated as

$\varepsilon_m \sim (\zeta/L')^\beta$, where the exponent β is either $1/2$ for $\varepsilon_m < \zeta/L'$, or $2/3$ for $\varepsilon_m > \zeta/L'$.

For unsteady wetting on soft surfaces, the defect size is not constant due to size variation of wetting ridges. The growth of the wetting ridge near the depinning moment can be expressed using Kelvin-Voigt model²⁵ as $\zeta = l[1 - \exp(-\delta t/\tau_v)]$ for $0 < \delta t \lesssim \Delta t$. Since the forcing duration δt during CL pinning is a few orders of magnitude smaller than the viscoelastic relaxation time, i.e., $\delta t \ll \tau_v$, we simplify the expression for ζ using Taylor expansion as $\zeta \approx l(\delta t/\tau_v)$. Using this expression for the defect size leads to a modified pinning force (per unit length) near the depinning moment for soft wetting:

$$f_p \sim k_r \left(\frac{l}{L'} \right)^\beta \left(\frac{\delta t}{\tau_v} \right)^\beta. \quad (4)$$

Here, we note that k_r is reasonably considered as a time-independent parameter for $0 < \delta t \lesssim \Delta t$. We highlight that by setting $\beta = \alpha$ and $k = k_r(l/L')^\alpha$, Eq. 4 yields the expression for the pinning force (per unit length) used in our calculation of the depinning condition for soft wetting

$$f_p \sim k \left(\frac{\delta t}{\tau_v} \right)^\alpha. \quad (5)$$

The time-independent constant k , herein referred to as the CL *soft spring constant*, is related to the material properties of the involved phases. A direct consequence of the relation between k and its rigid counter-part k_r (noting that typically $l/L' < 1$) is that soft surfaces most likely have lower spring constant – or higher contact angle hysteresis – than that on rigid surfaces. Moreover, we can safely assume that the maximum deformation of the liquid-air interface $\varepsilon_m L'$ is much larger than the defect size ζ of soft solid. As a result, we obtain $\varepsilon_m > \zeta/L'$, or $\varepsilon_m > \zeta/L'$, which leads to $\beta = 2/3$ ²⁶, consistent with our experimentally determined exponent $\alpha = 0.65 \pm 0.07$.

Conclusion

From our experiments of unsteady wetting on soft solids and the accompanying theoretical analysis, we find that unsteady wetting on soft solids exhibits intermittent spreading behaviour, i.e., the contact line (CL) alternates between sticking and slipping, when the liquid's spreading rate becomes comparable to the soft solid's viscoelastic reacting rate. During intermittent spreading, the contact line slips or sticks following the winning factor between the liquid's inertia and the pinning force at the contact line. Setting the transient inertia of the liquid during CL pinning equal to the opposing pinning force that grows at the same rate as the solid's viscoelastic characteristic timescale, we obtain the predictive condition for CL depinning, including the maximum time and the maximum contact angle increase allowed during CL pinning. This is experimentally verified and further supported by a modification of the classical theory for CL pinning on undeformable surfaces, treating the growing wetting ridge as dynamic surface heterogeneities.

Methods

Fabrication and characterization of soft surfaces. Soft surfaces were fabricated using PDMS (Polydimethylsiloxane, Sylgard 184, Dow) with the polymer-crosslinker weight ratios: 9:1, 10:1, 20:1, 30:1, 40:1, and 60:1. First, a PDMS mixture was prepared, stirred using a magnetic stirrer for 30 minutes, and degassed in a vacuum chamber for 60 minutes. The degassed mixture was coated on freshly cleaned microscope glass slides (Witeg) using a spin coater (POLOS 200, SPS) at a spin rate 2000 rounds-per-minute (RPM) for one minute to obtain a coating thickness of $75\ \mu\text{m}$. The

PDMS substrate was finally cured in an oven at 70° for 8 hours. The elastic properties of fabricated soft substrates were characterised using a rheometer (Discovery HR-20, TA Instruments). The surface roughness was measured by an atomic force microscope (AFM, Bruker)

Unsteady wetting experiment and imaging. We use DI water and ethanol-water mixtures as our working liquids. The schematic of the experimental setup is provided in the Supplementary Fig. 8. Droplets were generated at the tip of a stainless steel needle by injecting the liquid at a small rate ($1\mu\text{L min}^{-1}$). When the radius of a droplet reached $r_0 = 0.5\text{ mm}$, its lower surface gently touched a soft surface and the liquid started spreading. The spreading dynamics was recorded from the side using a high-speed camera (SA-X2, Photron) running at 50,000 frames per second (FPS), with back illumination provided by a diffused metal halide light source (LS-M180, Sumita). The side-view camera was equipped with a 20X long-working-distance objective (M-Plan Apo 20X, Optem Engineering), providing a resolution of $1\mu\text{m}/\text{pixel}$. Bottom-view interferometric recordings of the wetting ridge were obtained by a high-speed camera (SA-X2, Photron) imaging at 50,000 FPS. The camera was coupled with a 20X objective, providing a resolution of $0.9\mu\text{m}/\text{pixel}$. Coaxial illumination was provided by a green laser of wavelength $\lambda = 532\text{ nm}$ and a beam-splitter. The interferometric patterns indicating surface deformation, i.e., the wetting ridge were formed by reflected light from the the glass-PDMS interface and the PDMS-air interface on the dry side of the contact line. From the recorded interferometric patterns, deformation caused by the wetting ridge outside of the liquid droplet is reconstructed.

Determination of contact radius and contact angle. In side-view recordings of spreading droplets, the two points representing the CL positions on the side of a droplet are those where the air-liquid interface appears to intersect with the solid surface. These two points, herein referred to as side-view contact-line points (or side CL points), are used to obtain the contact radius r and its time dependence.

We note that the contact line in realistic wetting situations often does not stick nor slip synchronously. Tracking the side CL points is essentially tracking the faster-moving points of the contact line within the observing volume of the lens used to obtain the side-view images. This is consistent with our experimental observations showing that even during sticking, the velocity v_p of the side CL points never falls to zero. This also implies a small fluctuation of the contact angle θ along the contact line at any given time; and a non-zero deviation between θ and the contact angle θ_m measured from side-view recordings. The deviation between θ and θ_m is negligible during slipping, but it is significant during sticking where the side CL point appears moving slowly with velocity v_p while its neighboring points are pinned and not observable from the side view (Fig. 3a). It is possible to relate θ to θ_m during sticking as follows:

$$\tan \theta = \frac{v_c}{v_c - v_p \tan \theta_m} \tan \theta_m. \quad (6)$$

Flow velocity near contact line. We note a distinction between the contact line velocity v and the fluid flow velocity v_f near the contact line, i.e., v is the instantaneous CL velocity resulted from a complex interaction between flow inertia, capillary force, and the surface's elasticity at the contact line, whereas v_f is only governed by the flow inertia accumulated in the fast initial

spreading stage. The dependence of v_f on the initial flow inertia is consistent with the observation that the spreading radius strictly obeys the power law $r \sim t^b$ in the initial fast spreading stage and subsequently fluctuates around this law in the stick-slip stage due to the alternative stick-slip cycles²⁹. As a result, we define the flow velocity $v_f = C_0 t^{b-1}$ as the one characterising the flow inertia accumulated in the fast initial spreading stage. Here, the exponent b , varying from 0.25 to 0.3, results from fitting the power law to the data²⁹; the constant C_0 , varying from 1.4×10^{-3} to 2.5×10^{-3} , is determined for each spreading experiment using the least-square fitting method.

Critical Weber number for unsteady stick-slip behaviour. There exists a critical Weber number, denoted as We_c , separating the quasi-static stick-slip and unsteady stick-slip flow behaviours. The critical Weber number is estimated when the ridge's growing duration during pinning, Δt is comparable to the visco-elastic relaxation timescale τ_v of the solid. As a result, by setting $\Delta t = \tau_v$ in Eq. 2, we obtain

$$We_c \sim \left(\frac{\tau_c}{\tau_v} \Phi \right)^{1-\alpha} = \frac{k}{\pi \gamma \sin^2 \theta_p} \frac{\tau_c}{\tau_v}. \quad (7)$$

Subsequently, using the expression for soft spring constant $k \sim \pi \gamma \sin^2 \theta_p (l/L')^\alpha [\ln(L'/\zeta)]^{-1}$, we obtain an explicit expression of the critical Weber number:

$$We_c \sim [\ln(L'/\zeta)]^{-1} \left(\frac{l}{L'} \right)^\alpha \frac{\tau_c}{\tau_v}. \quad (8)$$

Our experimental data shows that $We_c \approx 0.0234 \pm 0.006$ for the explored range of shear modulus. This translates to the critical flow velocity $v_{f,c} \approx 57.9 \pm 8$ mm/s. The shaded areas in Fig. 2 and Fig. 4 respectively represent the critical velocity and the critical Weber number, consistent with the experimentally observed transitions between quasi-static and unsteady stick-slip regimes.

References

1. Jones, R. A. L. *Soft condensed matter*, vol. 6 (Oxford University Press, 2002).
2. Truby, R. L. & Lewis, J. A. Printing soft matter in three dimensions. *Nature* **540**, 371–378 (2016).
3. Park, S.-J. *et al.* Phototactic guidance of a tissue-engineered soft-robotic ray. *Science* **353**, 158–162 (2016).
4. Ma, M., Guo, L., Anderson, D. G. & Langer, R. Bio-inspired polymer composite actuator and generator driven by water gradients. *Science* **339**, 186–189 (2013).
5. Kato, T., Mizoshita, N. & Kishimoto, K. Functional liquid-crystalline assemblies: self-organized soft materials. *Angew. Chem. Int. Ed.* **45**, 38–68 (2006).
6. Zhao, X. *et al.* Active scaffolds for on-demand drug and cell delivery. *Proc. Nat. Acad. Sci.* **108**, 67–72 (2011).
7. Fusco, S. *et al.* An integrated microrobotic platform for on-demand, targeted therapeutic interventions. *Adv. Mater.* **26**, 952–957 (2014).
8. Lester, G. Contact angles of liquids at deformable solid surfaces. *J. Colloid Interface Sci.* **16**, 315–326 (1961).
9. Lester, G. Contact angles of liquids on organic solids. *Nature* **209**, 1126 (1966).

10. Style, R. W., Jagota, A., Hui, C.-Y. & Dufresne, E. R. Elastocapillarity: surface tension and the mechanics of soft solids. *Annu. Rev. Cond. Mat. Phys.* **8**, 99–118 (2017).
11. Chen, L. *et al.* Static and dynamic wetting of soft substrates. *Curr. Op. Colloid Interface Sci.* (2017).
12. Andreotti, B. & Snoeijer, J. H. Statics and dynamics of soft wetting. *Annu. Rev. Fluid Mech.* **52**, 285–308 (2020).
13. Style, R. W. *et al.* Universal deformation of soft substrates near a contact line and the direct measurement of solid surface stresses. *Phys. Rev. Lett.* **110**, 066103 (2013).
14. Gerber, J., Lendenmann, T., Eghlidi, H., Schutzius, T. M. & Poulikakos, D. Wetting transitions in droplet drying on soft materials. *Nat. Commun.* **10**, 1–10 (2019).
15. Kajiya, T. *et al.* Advancing liquid contact line on visco-elastic gel substrates: stick-slip vs. continuous motions. *Soft Matter* **9**, 454–461 (2013).
16. Kajiya, T. *et al.* A liquid contact line receding on a soft gel surface: dip-coating geometry investigation. *Soft Matter* **10**, 8888–8895 (2014).
17. van Gorcum, M., Andreotti, B., Snoeijer, J. H. & Karpitschka, S. Dynamic solid surface tension causes droplet pinning and depinning. *Phys. Rev. Lett.* **121**, 208003 (2018).
18. Park, S., Bostwick, J., De Andrade, V. & Je, J. Self-spreading of the wetting ridge during stick-slip on a viscoelastic surface. *Soft Matter* **13**, 8331–8336 (2017).

19. Guan, D., Charlaix, E. & Tong, P. State and rate dependent contact line dynamics over an aging soft surface. *Phys. Rev. Lett.* **124**, 188003 (2020).
20. Biance, A.-L., Clanet, C. & Quéré, D. First steps in the spreading of a liquid droplet. *Phys. Rev. E* **69**, 016301 (2004).
21. Winkels, K. G., Weijs, J. H., Eddi, A. & Snoeijer, J. H. Initial spreading of low-viscosity drops on partially wetting surfaces. *Phys. Rev. E* **85**, 055301 (2012).
22. Chen, L., Bonaccorso, E. & Shanahan, M. E. Inertial to viscoelastic transition in early drop spreading on soft surfaces. *Langmuir* **29**, 1893–1898 (2013).
23. Karpitschka, S. *et al.* Droplets move over viscoelastic substrates by surfing a ridge. *Nat. Commun.* **6**, 7891 (2015).
24. Varagnolo, S. *et al.* Stick-slip sliding of water drops on chemically heterogeneous surfaces. *Phys. Rev. Lett.* **111**, 066101 (2013).
25. Ward, I. M. & Sweeney, J. *An introduction to the mechanical properties of solid polymers* (John Wiley & Sons, 2004).
26. Joanny, J. & De Gennes, P.-G. A model for contact angle hysteresis. *J. Chem. Phys.* **81**, 552–562 (1984).
27. Bonn, D., Eggers, J., Indekeu, J., Meunier, J. & Rolley, E. Wetting and spreading. *Rev. Mod. Phys.* **81**, 739 (2009).

28. Vo, Q. & Tran, T. Critical conditions for jumping droplets. *Phys. Rev. Lett.* **123**, 024502 (2019).
29. Chen, L., Auernhammer, G. K. & Bonaccorso, E. Short time wetting dynamics on soft surfaces. *Soft Matter* **7**, 9084–9089 (2011).

Acknowledgements This study is supported by Nanyang Technological University, the Republic of Singapore’s Ministry of Education (MOE, Grant No. MOE2018-T2-2-113), and the RIE2020 Industry Alignment Fund – Industry Collaboration Projects (IAF-ICP) Funding Initiative, as well as cash and in-kind contribution from the industry partner, HP Inc. S.M. is supported by NTU Research Scholarship. M.L. is supported by Nanyang President’s Graduate Scholarship.

Author contributions statement T.T. conceived the study. S.M. and Q.V. performed the experiment and analysed the data with assistance from M.L. S.M., Q.V., and T.T. discussed the results, T.T. wrote the manuscript with inputs from S.M., Q.V., and M.L.; T.T. supervised the research.

Competing Interests The authors declare that they have no competing financial interests.

Correspondence Correspondence and requests for materials should be addressed to Tuan Tran (email: ttran@ntu.edu.sg),